Research Square

Preprints are preliminary reports that have not undergone peer review.
They should not be considered conclusive, used to inform clinical practice,
or referenced by the media as validated information.

MRI-Based Morphologic Patterns Associated With Lateral Patellar Dislocation: An Interpretable Machine Learning Retrospective Case–Control Study

Jianhong Zhou
The First Affiliated Hospital of Kunming Medical University
Minyuan Zhang
The First Affiliated Hospital of Kunming Medical University
Jinyu Zhang
The First Affiliated Hospital of Kunming Medical University
Lizhi Peng
The First Affiliated Hospital of Kunming Medical University
Xianguang Yang
The First Affiliated Hospital of Kunming Medical University
Guofeng Cai
34763623@qq.com

The First Affiliated Hospital of Kunming Medical University

Research Article

Keywords: lateral patellar dislocation, magnetic resonance imaging, osseous morphology, interpretable machine learning, SHAP, nonlinear association

Posted Date: September 28th, 2026

DOI: https://doi.org/10.21203/rs.3.rs-10945170/v1

License: This work is licensed under a Creative Commons Attribution 4.0 International License.
Read Full License

Additional Declarations: No competing interests reported.

Abstract

Background

To identify nonlinear associations and threshold-like patterns between MRI-derived osseous morphology and lateral patellar dislocation using Shapley additive explanations (SHAP).

Methods

This retrospective case–control study included 446 knees: 198 with lateral patellar dislocation and 248 symptomatic controls without patellar instability. Ten patellofemoral morphologic parameters were assessed. The cohort was stratified into training (70%) and testing (30%) sets. Features were selected using least absolute shrinkage and selection operator regression and 500 bootstrap resamples. Nine machine-learning models were developed using stratified 10-fold cross-validation and evaluated in the independent testing set. The best-performing model was interpreted using SHAP analyses.

Results

Seven features were retained for modeling. Random forest achieved the best overall performance, with area under the receiver operating characteristic curve values of 0.997 in out-of-fold evaluation and 1.000 in independent testing. SHAP analysis identified trochlear groove depth (TGD), Insall–Salvati index (ISI), and sulcus angle (SA) as the most influential features. Lower TGD, higher ISI, and larger SA shifted model outputs toward patellar dislocation. Their contributions were nonlinear, with prominent transitions at approximately 3.0–3.6 mm, 1.15–1.40, and 143°–151°, respectively.

Conclusions

SHAP-based interpretable machine learning revealed nonlinear morphologic patterns associated with lateral patellar dislocation, predominantly involving trochlear depth, patellar height, and trochlear configuration. These transition regions provide anatomical insights but should not be regarded as validated diagnostic thresholds.

Background

Lateral patellar dislocation is a common knee injury in adolescents and young adults[1]. Patellar stability is maintained by the combined effects of osseous anatomy, lower-extremity alignment, and soft-tissue restraints. Abnormality in any component can alter patellofemoral stability. Consequently, lateral patellar dislocation is generally not attributable to a single anatomical abnormality but reflects the combined influence of multiple predisposing factors[2]. Identifying the morphologic features associated with

patellar dislocation may clarify its anatomical basis and improve the focus of MRI evaluation in patients with suspected patellofemoral instability.

Trochlear dysplasia, patella alta, lateral patellar tilt, and tibial tubercle lateralization are recognized anatomical correlates of lateral patellar dislocation[2,3]. MRI can depict patellofemoral cartilage, the medial patellofemoral ligament, and associated injuries while also permitting quantitative assessment of trochlear morphology, patellar height, and extensor-mechanism alignment[4,5]. Lateral trochlear inclination, trochlear groove depth, trochlear facet asymmetry, sulcus angle, the Insall–Salvati index, Caton–Deschamps index, patellotrochlear index, patellar tilt angle, and TT–TG distance have all been used to characterize patellofemoral morphology. However, these measurements are anatomically correlated, and their associations with patellar dislocation may be nonlinear. Single-parameter cutoffs and conventional linear models may therefore incompletely represent their combined morphologic pattern.

Recent MRI-based machine-learning studies have attempted to integrate multiple patellofemoral morphologic measurements rather than relying on a single conventional cutoff. SHAP provides a model-agnostic framework for quantifying feature contributions at both the global and individual-prediction levels[6]. Nukala et al. evaluated MRI measures of patellar height, including the Insall–Salvati ratio, modified Insall–Salvati ratio, Caton–Deschamps index, Blackburne–Peel index, and patellotrochlear index; extensor-mechanism alignment measures, including tibial tubercle–trochlear groove (TT–TG), anteroposterior TT–TG, and tibial tubercle–posterior cruciate ligament distances; and trochlear morphologic measures, including trochlear depth, sulcus angle, and lateral trochlear inclination.Logistic regression, decision tree, and random forest models were compared, with random forest achieving the highest discrimination (AUC, 0.85). SHAP was used to report global and local feature importance, identifying the Insall–Salvati ratio, TT–TG distance, and trochlear depth as the leading variables; however, the model was developed from a single-institution cohort without external validation, and the study did not systematically characterize feature-specific changes in SHAP contribution across the continuous range of each measurement[7]. Kwon et al. assessed 10 MRI morphologic parameters, including trochlear depth, sulcus angle, trochlear facet asymmetry, lateral trochlear inclination, trochlear groove medialization, patellar shape parameters, patellar tilt, and the Insall–Salvati ratio. They compared logistic regression, support vector machine, and LightGBM models with genetic-algorithm-based feature optimization; optimized LightGBM achieved the highest AUC (0.873). Their evaluation was based on cross-validation, without external validation or SHAP-based interpretation[8]. Using a different 3-dimensional MRI statistical shape-analysis approach, Nagawa et al. compared linear discriminant analysis, linear and radial-basis-function support vector machines, k-nearest neighbors, and random forest classifiers. Linear support vector machine achieved an AUC of 0.939 in five-fold cross-validation; however, this model was based on femoral shape components rather than routinely measured clinical MRI parameters and did not use SHAP or external validation[9]. Therefore, although previous studies have demonstrated that machine learning can distinguish patellofemoral instability from control knees and can rank influential morphologic variables, resampling-based assessment of feature-selection

stability, systematic evaluation of the direction of model contribution, and characterization of nonlinear transition regions across continuous MRI measurements remain insufficiently explored.

This study therefore measured 10 MRI-derived patellofemoral morphologic parameters and compared nine supervised machine-learning algorithms to identify patterns associated with lateral patellar dislocation. Rather than merely ranking variables according to their association with lateral patellar dislocation, the primary aim was to use SHAP-based interpretable machine learning to characterize nonlinear, value-dependent patterns in model contribution. The best-performing model was interpreted using SHAP to identify the ranges over which key morphologic features shifted the model output most prominently toward or away from lateral patellar dislocation. These transition regions were interpreted as hypothesis-generating model-derived patterns rather than validated clinical thresholds. The study was designed to classify knees according to existing lateral patellar dislocation status rather than to predict a future first dislocation or subsequent recurrence.

Methods

The study was approved by the institutional ethics committee and conducted in accordance with the ethical principles of the Declaration of Helsinki. This retrospective case–control study screened 1,512 patients who underwent knee magnetic resonance imaging (MRI) between December 2022 and April 2026. A total of 446 affected knees were ultimately included, comprising 198 knees with a documented history of lateral patellar dislocation and 248 symptomatic control knees (Fig. 1). The inclusion criteria were patients with a clinically confirmed diagnosis of lateral patellar dislocation and available knee MRI data, as well as patients who underwent MRI for knee pain but had no history or clinical evidence of patellar dislocation or patellofemoral instability. Patellar dislocation was defined as an event in which the patella completely disengaged from the femoral trochlea and was subsequently reduced either spontaneously or with physician assistance[10].

The exclusion criteria were as follows: (1) a history of knee or patellofemoral surgery; (2) severe motion artifacts or inadequate visualization of the anatomical landmarks required for MRI measurements; (3) concomitant fracture, tumor, infection, inflammatory arthropathy, or other conditions that could substantially alter patellofemoral morphology; and (4) incomplete clinical data or missing key MRI-based morphologic measurements.

The patellar dislocation group comprised 198 knees with lateral patellar dislocation, whereas the remaining 248 knees constituted the symptomatic control group. Ten MRI-based anatomical parameters were measured and analyzed: lateral trochlear inclination (LTI), trochlear groove depth (TGD), trochlear facet asymmetry (TFA), sulcus angle (SA), patellotrochlear index (PTI), Caton–Deschamps index (CDI), Insall–Salvati index (ISI), patellar tilt angle (PTA), tibial tubercle–trochlear groove distance (TT–TG), and tibial tubercle–midepicondyle distance (TT–ME). These parameters were used to identify anatomical features associated with lateral patellar dislocation and to develop machine-learning models for distinguishing knees with patellar dislocation from symptomatic control knees.

Data collection

Demographic and clinical information was obtained from the electronic medical record, including age, sex, body mass index (BMI), and affected side. In the dislocation group, the interval between MRI and the dislocation event was also recorded. All MR examinations were obtained after patellar reduction. When both knees met the eligibility criteria, only the side evaluated at the first visit was included so that each patient contributed one study unit.

All knee MR images were retrieved from the institutional picture archiving and communication system (PACS).Examinations were performed using a Siemens 3.0-T scanner and a dedicated 8-channel knee coil with a section thickness of 1.5 mm. Patients were positioned supine with the knee extended and the quadriceps relaxed.

Ten MRI-derived patellofemoral morphologic parameters were measured: lateral trochlear inclination (LTI), trochlear groove depth (TGD), trochlear facet asymmetry (TFA), sulcus angle (SA), patellotrochlear index (PTI), Caton–Deschamps index (CDI), Insall–Salvati index (ISI), patellar tilt angle (PTA), tibial tubercle–trochlear groove distance (TT–TG), and tibial tubercle–midepicondyle distance (TT–ME). All variables were analyzed continuously and were not dichotomized according to previously proposed cutoff values.

LTI was measured using two axial MR images. A posterior condylar reference line was drawn on an image approximately 3 cm proximal to the tibiofemoral joint line where the posterior margins of both femoral condyles were clearly visible. A second line was drawn along the subchondral bone of the lateral trochlear facet on the most proximal image showing complete trochlear cartilage. After projection into a common coordinate system, the angle between these lines was recorded as LTI[11].(figure 2)

TGD, TFA, and SA were measured on the same axial image, approximately 3 cm proximal to the tibiofemoral joint line, showing the deepest point of the trochlear groove, complete medial and lateral trochlear facets, and a Roman-arch configuration of the distal femur. The subchondral bone contour served as the anatomical landmark for all trochlear measurements[2,12].(figure 2)

For TGD, the posterior condylar line served as the reference. Perpendicular distances from this line to the most anterior points of the medial and lateral trochlear facets and to the deepest point of the groove were designated M, L, and G, respectively. TGD was calculated as (M + L)/2 − G and expressed in millimeters.

TFA was calculated as the length of the medial trochlear facet divided by the length of the lateral trochlear facet and multiplied by 100%. Each facet length was measured from the deepest point of the trochlear groove to the most anterior point of the corresponding facet.

SA was defined as the angle formed by tangential lines drawn along the medial and lateral trochlear facets[2].

PTI, CDI, and ISI were measured on a sagittal image that clearly demonstrated the maximum longitudinal axis of the patella, the complete patellar articular surface, and the tibial insertion of the patellar tendon[3].(figure 3)

PTI quantified sagittal overlap between patellar and trochlear articular cartilage. The longitudinal length of the patellar articular cartilage was designated P, and the length overlapping the trochlear cartilage was designated F. PTI was calculated as F/P[13].

CDI was calculated as the distance from the anterosuperior margin of the tibial plateau to the inferior margin of the patellar articular cartilage divided by the length of the patellar articular surface.

ISI was calculated as patellar tendon length divided by osseous patellar length. Tendon length was measured from the inferior pole of the patella to the tibial tubercle insertion, and patellar length was the greatest distance between the superior and inferior poles[3].

PTA was measured on two axial images. The posterior condylar line was drawn where the posterior margins of both femoral condyles were clearly visible, and the maximum transverse patellar axis was drawn on the image showing the greatest patellar width. After projection into a common coordinate system, the angle between these lines was recorded as PTA[14].(figure 4)

TT–TG distance was measured using two axial images. The deepest point of the trochlear groove was identified relative to the posterior condylar line, and the midpoint of the patellar tendon insertion was identified at the tibial tubercle. After image superimposition, perpendicular lines were drawn through both points; their transverse separation was recorded as TT–TG distance[15].(figure 4)

TT–ME distance was measured according to the geometric method described by Iseki et al[16]. The transepicondylar line was drawn between the most prominent medial and lateral epicondylar points, and its midpoint was determined. After superimposition with the axial image showing the highest point of the tibial tubercle, the transverse distance between the midpoint of the transepicondylar line and the tibial tubercle was recorded as TT–ME distance. The original CT-based anatomical landmarks and geometric principle were applied to MRI in the present study.(figure 4)

Observer reliability

To assess measurement reproducibility, 50 knees were randomly selected from the overall cohort. Two observers independently measured all 10 MRI-based morphologic parameters using the standardized protocol, and one observer repeated the measurements after an interval of at least 2 weeks. Interobserver and intraobserver reliability were assessed using intraclass correlation coefficients with 95% confidence intervals, calculated using a two-way random-effects model with absolute agreement for single measurements [ICC(2,1)].

Statistical analysis and model development

All analyses were performed using R software (version 4.4.1; R Foundation for Statistical Computing, Vienna, Austria). The cohort was stratified by outcome and randomly divided into a training set (70%) and an independent testing set (30%). The testing set remained isolated during feature selection and model development and was used only for final evaluation. Continuous variables are presented as mean ± standard deviation or median (interquartile range) and were compared using the independent-samples *t* test or Mann–Whitney *U* test, as appropriate. Categorical variables are presented as counts and percentages and were compared using the Pearson chi-square test or Fisher exact test. All tests were two-sided, with $P < .05$ indicating statistical significance.

Feature selection was performed in the training set using least absolute shrinkage and selection operator (LASSO) logistic regression with stratified 10-fold cross-validation. Candidate features were defined as variables with nonzero coefficients at the one-standard-error penalty parameter (λ.1se). Selection stability was subsequently assessed by repeating the LASSO procedure in 500 bootstrap resamples. A selection frequency of ≥ 70% indicated relatively stable selection. Variables with slightly lower frequencies could be retained based on previous evidence and biomechanical relevance. The final feature set included trochlear groove depth (TGD), trochlear facet asymmetry (TFA), sulcus angle (SA), Caton–Deschamps index (CDI), Insall–Salvati index (ISI), patellar tilt angle (PTA), and tibial tubercle–trochlear groove distance (TT–TG).

Nine supervised machine-learning models were developed using these features: Light Gradient Boosting Machine, CatBoost, gradient boosting machine, support vector machine, random forest, naïve Bayes, extreme gradient boosting, neural network, and decision tree. Model training and hyperparameter optimization were performed using stratified 10-fold cross-validation. Performance was assessed using the area under the receiver operating characteristic curve, accuracy, sensitivity, specificity, positive predictive value, negative predictive value, and F1 score. Out-of-fold cross-validation performance was used for model comparison, and the independent testing set was used for final internal validation. The model with the most favorable overall performance was selected for interpretation.

SHAP-based model interpretation

The final model was interpreted using Shapley additive explanations (SHAP), a framework derived from cooperative game theory that decomposes each model output into feature-specific contributions relative to the expected model output. For an individual knee, a positive SHAP value indicates that the feature shifts the model output toward lateral patellar dislocation, whereas a negative value shifts it toward the symptomatic control group. The absolute SHAP value represents the magnitude of that contribution.

Global feature importance was quantified by the mean absolute SHAP value across all observations. SHAP beeswarm plots were used to show the magnitude and direction of feature contributions together with the distribution of feature values. Dependence plots were generated for the three most influential

variables—TGD, ISI, and SA—to characterize nonlinear and threshold-like relationships between their observed values and model output. SHAP values reflect how the fitted model uses each feature and should not be interpreted as conventional regression coefficients, causal effects, or validated clinical thresholds. Therefore, abrupt changes in SHAP values were regarded as model-derived transition regions that may provide anatomical insights rather than definitive diagnostic cutoff values.

Results

Group comparisons in the training set

The differences in demographic and imaging characteristics between patients with and without patellar dislocation in the training set are summarized in Table 1. Compared with the control group, the patellar dislocation group was significantly younger (20.99 ± 8.54 vs. 33.82 ± 10.18 years, $P < 0.001$) and had a higher proportion of female participants (77.6% vs. 52.5%, $P < 0.001$). Regarding imaging characteristics, the patellar dislocation group showed significantly lower LTI (10.89 ± 5.49° vs. 17.86 ± 3.66°), TGD (2.20 ± 0.81 vs. 4.56 ± 0.80 mm), and TFA (41.01 ± 11.22 vs. 57.53 ± 8.52), together with a greater SA (154.10 ± 8.44° vs. 139.35 ± 4.78°; all $P < 0.001$). The patellar dislocation group also had significantly greater CDI (1.313 ± 0.167 vs. 1.039 ± 0.113), ISI (1.333 ± 0.206 vs. 1.031 ± 0.096), PTA (22.97 ± 9.64° vs. 8.00 ± 4.83°), TT–TG distance (13.59 ± 4.38 vs. 7.71 ± 3.30 mm), and TT–ME distance (12.30 ± 4.29 vs. 7.22 ± 3.31 mm; all $P < 0.001$). No significant between-group differences were observed in affected-side distribution, BMI, or PTI (all $P > 0.05$).

Table 1
Baseline demographic and imaging characteristics of the training set

Variable	Patellar dislocation		*P*-value
	No (*n* = 179)	Yes (*n* = 134)	
Sex, n (%)			**< 0.001**
Male	85 (47.5)	30 (22.4)	
Female	94 (52.5)	104 (77.6)	
Age, years	33.82 ± 10.18	20.99 ± 8.54	**< 0.001**
Affected side, n (%)			0.234
Left	95 (53.1)	62 (46.3)	
Right	84 (46.9)	72 (53.7)	
LTI, °	17.86 ± 3.66	10.89 ± 5.49	**< 0.001**
TGD, mm	4.56 ± 0.80	2.20 ± 0.81	**< 0.001**
TFA, %	57.53 ± 8.52	41.01 ± 11.22	**< 0.001**
SA, °	139.35 ± 4.78	154.10 ± 8.44	**< 0.001**
PTI	0.351 ± 0.122	0.362 ± 0.150	0.491
CDI	1.039 ± 0.113	1.313 ± 0.167	**< 0.001**
ISI	1.031 ± 0.096	1.333 ± 0.206	**< 0.001**
PTA, °	8.00 ± 4.83	22.97 ± 9.64	**< 0.001**
TT–TG distance, mm	7.71 ± 3.30	13.59 ± 4.38	**< 0.001**
TT–ME distance, mm	7.22 ± 3.31	12.30 ± 4.29	**< 0.001**
BMI, kg/m²	24.19 ± 3.90	23.41 ± 4.54	0.103

Note: Continuous variables are presented as mean ± standard deviation, and categorical variables as number (percentage). Percentages were calculated within each patellar dislocation group. Between-group comparisons were performed using independent-samples *t* tests for continuous variables and Pearson's chi-square tests for categorical variables. For PTI, Welch's *t* test was used because the assumption of homogeneity of variance was not met. **Bold** values indicate statistical significance ($P < 0.05$).

Abbreviations: BMI, body mass index; CDI, Caton–Deschamps index; ISI, Insall–Salvati index; LTI, lateral trochlear inclination; PTA, patellar tilt angle; PTI, patellotrochlear index; SA, sulcus angle; TFA, trochlear

facet asymmetry; TGD, trochlear groove depth; TT–ME, tibial tubercle–midepicondyle distance; TT–TG, tibial tubercle–trochlear groove distance.

Observer reliability

Interobserver and intraobserver reliability were good to excellent for all MRI-based morphologic measurements. Interobserver ICCs ranged from 0.82 to 0.94, and intraobserver ICCs ranged from 0.87 to 0.96.

LASSO feature selection and bootstrap stability

Using the one-standard-error criterion (λ.1se), LASSO regression identified seven variables with nonzero coefficients in the training set: TGD, TFA, SA, CDI, ISI, PTA, and TT–TG distance. The 10-fold cross-validation curve used to determine λ and the corresponding LASSO coefficient profiles are presented in Fig. 5. To further assess the reproducibility of variable selection, the LASSO procedure was repeated across 500 bootstrap resamples. TGD and ISI were selected in all resamples (100.0%), followed by SA (98.2%), CDI (97.4%), and TT–TG distance (82.2%). These five variables exceeded the prespecified 70% selection-frequency threshold and were therefore considered the relatively stable, data-driven feature set.

PTA and TFA were selected in 64.8% and 64.6% of the bootstrap resamples, respectively, indicating more moderate selection stability. The selection frequency then decreased markedly to 38.8% for the next-ranked variable, PTI, and remained below 40% for all other candidate variables. The complete bootstrap stability results are presented in Supplementary Fig. 1 and Supplementary Table 1. Accordingly, TGD, ISI, SA, CDI, and TT–TG distance constituted the stable LASSO-derived feature set. TFA and PTA were retained as clinically informed candidate variables for subsequent model development because previous patellofemoral instability research and biomechanical evidence support the relevance of trochlear geometry and patellar tilt to patellar dislocation.

Model development and comparison

Seven variables—TGD, TFA, SA, CDI, ISI, PTA, and TT–TG distance—were included using a combined data-driven and knowledge-informed strategy. TGD, ISI, SA, CDI, and TT–TG distance were retained as stable LASSO-derived features, with selection frequencies exceeding 70% across 500 bootstrap resamples. TFA and PTA were additionally retained based on previous evidence and their biomechanical relevance to trochlear morphology and patellar alignment.

Nine machine learning models were developed using the same seven variables: LightGBM, CatBoost, gradient boosting machine, support vector machine, random forest (RF), naive Bayes, XGBoost, neural network, and decision tree. Their out-of-fold and independent testing-set performance is presented in

Tables 2 and 3, respectively, and the ROC curves for the training-set resubstitution, 10-fold out-of-fold, and testing analyses are shown in Fig. 6A–C.

Table 2
Out-of-fold performance of the nine machine learning models in the training set

Model	AUC	Accuracy	Sensitivity	Specificity	F1 score
LightGBM	0.973	0.981	0.985	0.978	0.978
CatBoost	0.993	0.987	0.978	0.994	0.985
GBM	0.996	0.971	0.993	0.955	0.967
SVM	0.993	0.981	0.993	0.972	0.978
Random Forest	0.997	0.987	0.985	0.989	0.985
Naive Bayes	0.994	0.984	0.978	0.989	0.981
XGBoost	0.981	0.962	0.955	0.966	0.955
Neural Network	0.992	0.974	0.970	0.978	0.970
Decision Tree	0.968	0.978	0.978	0.978	0.974

Note: Model performance was evaluated using out-of-fold predictions generated through stratified 10-fold cross-validation in the training set. Each participant was evaluated by a model that had not been trained using that participant. Accuracy, sensitivity, specificity, and F1 score were calculated using model-specific probability cutoffs determined from the out-of-fold predictions by maximizing the Youden index. Patellar dislocation was defined as the positive class. All values are reported to three decimal places.

Abbreviations: AUC, area under the receiver operating characteristic curve; GBM, gradient boosting machine; SVM, support vector machine; XGBoost, extreme gradient boosting; F1, harmonic mean of precision and sensitivity; OOF, out-of-fold.

Table 3
Performance of the nine machine learning models in the independent testing set

Model	AUC	Accuracy	Sensitivity	Specificity	F1 score
LightGBM	0.990	0.970	0.984	0.957	0.969
CatBoost	1.000	0.985	0.984	0.986	0.984
GBM	0.998	0.940	1.000	0.884	0.941
SVM	0.998	0.955	1.000	0.913	0.955
Random Forest	1.000	0.970	1.000	0.942	0.970
Naive Bayes	0.995	0.970	1.000	0.942	0.970
XGBoost	0.996	0.977	0.984	0.971	0.977
Neural Network	0.999	0.955	0.984	0.928	0.955
Decision Tree	0.977	0.977	0.969	0.986	0.976

Note: Model performance was evaluated in the independent testing set, which was not used for model training, hyperparameter selection, or probability-cutoff determination. Accuracy, sensitivity, specificity, and F1 score were calculated using the corresponding model-specific cutoffs derived exclusively from the training-set out-of-fold predictions by maximizing the Youden index; no cutoff was re-estimated in the testing set. Patellar dislocation was defined as the positive class. All values are reported to three decimal places.
Abbreviations: AUC, area under the receiver operating characteristic curve; GBM, gradient boosting machine; SVM, support vector machine; XGBoost, extreme gradient boosting; F1, harmonic mean of precision and sensitivity; OOF, out-of-fold.

Out-of-fold AUCs ranged from 0.9682 to 0.9971. RF achieved the highest AUC of 0.9971 (95% CI, 0.9925–1.0000), with an accuracy of 0.987, sensitivity of 0.985, specificity of 0.989, and F1 score of 0.985. In the independent testing set, RF maintained an AUC of 1.0000, with an accuracy of 0.970, sensitivity of 1.000, specificity of 0.942, and F1 score of 0.970. Considering its highest out-of-fold AUC and consistently high discrimination across evaluation settings, RF was selected for subsequent SHAP-based interpretation.

Model explainability

SHAP-based interpretation of the RF model identified TGD as the dominant contributor to model output, followed by ISI and SA (Fig. 7A). The SHAP summary plot showed that lower TGD values were predominantly associated with positive SHAP contributions, whereas higher ISI and SA values shifted model predictions toward patellar dislocation (Fig. 7B). The SHAP dependence plot demonstrated a marked non-linear, threshold-like pattern for TGD: lower values produced positive contributions, followed by a rapid decline at approximately 3.0–3.6 mm and predominantly negative contributions at higher values (Fig. 8A). ISI also showed a non-linear pattern, with SHAP contributions increasing rapidly at

approximately 1.15–1.40 and remaining predominantly positive at higher values (Fig. 8B). Because TGD and SA both characterize trochlear development, their patterns were interpreted together. Lower TGD, reflecting a shallower trochlear groove, and higher SA, reflecting a flatter trochlear configuration, shifted model predictions toward patellar dislocation; the contribution of SA changed most rapidly at approximately 143°–151° (Fig. 8C). Collectively, these findings suggest that shallow and flattened trochlear morphology, together with increased patellar height, constituted the principal morphologic pattern used by the RF model to classify patellar dislocation. The transition ranges represent model-derived changes in SHAP contribution rather than validated clinical diagnostic cutoffs.

Discussion

Principal findings

The principal contribution of this study was not simply the identification of morphologic variables associated with lateral patellar dislocation. Instead, SHAP analysis was used to examine how the contribution of each key MRI-derived feature changed across its continuous range. This approach identified nonlinear, threshold-like transition regions for TGD, ISI, and SA, thereby extending conventional feature-importance ranking toward a value-dependent interpretation of patellofemoral morphology. Within a strictly separated training and internal holdout testing framework, this study evaluated MRI-derived morphologic features associated with lateral patellar dislocation. LASSO regression with bootstrap stability analysis identified TGD, ISI, SA, CDI, and TT–TG distance as relatively stable features; TFA and PTA were additionally retained because of prior evidence and biomechanical relevance. Among nine algorithms, RF showed consistently high discrimination in out-of-fold and internal holdout evaluations and was selected for interpretation. SHAP analysis ranked TGD first, followed by ISI and SA. Lower TGD, higher ISI, and larger SA shifted model output toward lateral patellar dislocation and displayed pronounced nonlinear changes across their continuous ranges.

These findings accord with the multifactorial anatomy of patellar instability. The trochlea provides osseous restraint, patellar height affects the timing of trochlear engagement during early flexion, and groove depth and configuration influence stability after engagement[2,17]. The leading variables should therefore be interpreted as a combined pattern of a shallow, flattened trochlea with a relatively high patella rather than as independent causal factors. SHAP further showed that model contributions changed rapidly within specific ranges rather than uniformly across observed values.

TGD and trochlear osseous restraint

TGD was the most influential model feature. It was lower in the dislocation group and was selected in every bootstrap resample, indicating a stable association with the study outcome in this dataset. This result is consistent with MRI studies identifying reduced trochlear depth as an important manifestation of trochlear dysplasia and patellofemoral instability[12,18].

A normal trochlear groove limits lateral patellar translation during knee flexion. A shallow groove weakens osseous containment and guidance, increasing reliance on medial soft-tissue restraints. When lateral force is applied or medial restraints are compromised, insufficient osseous restraint may further facilitate lateral translation.

TGD contributions changed rapidly at approximately 3.0–3.6 mm. Values below this range generally contributed toward dislocation, whereas higher values usually contributed toward the control class. Although this interval is close to the approximately 3-mm reference used to describe trochlear dysplasia[12], it represents a transition in RF model contribution, not an externally validated diagnostic threshold or a direct biomechanical critical value.

ISI and patellar height

ISI was the second most influential feature and was selected in every bootstrap resample. A relatively high patella delays engagement with the trochlea, leaving stability during early flexion more dependent on medial soft tissues. Before the trochlea provides effective osseous restraint, lateral forces may therefore more readily displace the patella. Previous studies have likewise identified patella alta as an important morphologic correlate of lateral patellar dislocation[3,17,18].

ISI contributions increased rapidly at approximately 1.15–1.40, and higher values generally shifted model output toward dislocation. The breadth of this interval argues against a simple binary relationship. Knees with similar ISI values may receive different contributions because of differences in trochlear morphology, patellar tilt, and tibial tubercle position. ISI should therefore be interpreted jointly with other morphologic measurements rather than as a stand-alone criterion.

SA and trochlear configuration

SA was the third most influential feature, was greater in the dislocation group, and was selected in 98.2% of bootstrap resamples. A larger SA reflects a flatter trochlear groove and complements the information represented by lower TGD. Prior imaging studies have also linked larger SA with trochlear dysplasia and patellofemoral instability[12,19].

SA contributions changed most prominently at approximately 143°–151°, with larger angles generally shifting output toward dislocation. This interval includes the commonly used reference of approximately 145°[2], but it does not establish a new clinical cutoff. Because TGD and SA characterize the same anatomical structure, their contributions may be correlated. SHAP importance reflects how the model uses variables within the observed feature set and cannot isolate independent biological effects. TGD and SA are therefore best interpreted together as a shallow and flattened trochlear configuration.

Roles of other morphologic features

CDI and TT–TG distance showed relatively high selection stability, supporting patellar height and tibial tubercle lateralization as components of the associated morphologic pattern. TFA and PTA were less stable but were retained on the basis of prior evidence and biomechanical relevance[3]. Their lower

SHAP contributions may reflect information overlap: TFA and SA both describe trochlear development, whereas PTA may be influenced by trochlear morphology, patellar position, and knee positioning during MRI.

Exclusion of LTI, PTI, and TT–ME from the final model does not imply that they are unrelated to patellofemoral stability. Feature selection estimates the additional information supplied by a variable in a specific dataset when other candidates are present; variables with similar anatomical meaning may be excluded because of collinearity or redundancy. TT–ME was originally proposed using CT with the knee extended[16]. Its cross-modality validity after application of the same geometric method to MRI requires further study.

Model performance and explainability

RF achieved high AUCs in both out-of-fold evaluation and the internal holdout test set, including an AUC of 1.000 in the latter. This may reflect marked morphologic separation between the dislocation and symptomatic control groups. Nevertheless, near-perfect internal discrimination requires caution. The holdout set was isolated from feature selection, training, and cutoff determination, but it originated from the same center and retrospective cohort and shared the same scanning and measurement procedures. Such homogeneity can yield performance estimates that exceed those obtained in other institutions or consecutive clinical populations[20].

SHAP improved interpretation beyond reporting AUC or a single feature-importance ranking by showing the direction and magnitude of contributions and their nonlinear dependence on continuous feature values. However, SHAP explains how a fitted model uses its inputs; it does not establish causality between a measurement and patellar dislocation[6]. A high SHAP contribution likewise does not demonstrate an independent biomechanical effect.

Clinical relevance and limits of interpretation

A shallow trochlear groove, relatively high patella, and flattened trochlear configuration jointly formed the principal MRI pattern associated with lateral patellar dislocation. These findings may encourage a systematic assessment of trochlear depth, patellar height, and trochlear configuration in patients with anterior knee pain or suspected patellofemoral instability rather than reliance on a single measurement.

The model should not presently be used as a stand-alone diagnostic tool. Groups were defined by existing lateral patellar dislocation status; thus, the model identifies MRI morphology associated with that status and does not prospectively predict a future dislocation. The SHAP transition regions should not determine conservative treatment, operative treatment, surgical technique, or indications. Their present value is to generate morphologic patterns and candidate ranges for subsequent validation.

Limitations and future directions

This study has several limitations. First, its single-center retrospective case–control design precludes causal inference and may introduce selection bias. Symptomatic controls underwent MRI for knee pain

and do not represent a healthy population, limiting generalizability to similar clinical populations. Conversely, this comparator may be more relevant than healthy volunteers to patients undergoing MRI for diagnostic evaluation.

Second, the groups differed in age and sex. Although the final model used only MRI morphologic measurements, age, sex, and skeletal maturity may be related to some parameters, and residual confounding cannot be excluded. Matching, stratified analyses, or multivariable adjustment should address these factors in future studies.

Third, the internal holdout test set was drawn from the same center and cannot replace external validation. Given its AUC of 1.000, future studies should evaluate discrimination, calibration, and clinical net benefit across institutions, MRI systems and protocols, and consecutively enrolled populations[20,21].

Fourth, MRI morphologic measurements depend on image selection and anatomical landmark identification and may be affected by observer experience and image quality [22]. TT–ME and other measurements transferred across imaging modalities also require MRI-specific reliability and validity assessment.

Finally, the TGD, ISI, and SA transition regions were derived from this model and sample distribution and may vary with population, imaging protocol, and model parameters. They should be replicated in external cohorts and evaluated using prespecified validation analyses, restricted cubic splines, or segmented regression.

Conclusions

This study used SHAP-based interpretable machine learning to identify nonlinear, value-dependent morphologic patterns associated with lateral patellar dislocation. Beyond identifying TGD, ISI, and SA as influential model features, SHAP dependence analyses demonstrated transition regions in their contributions to model output. These regions should be regarded as hypothesis-generating patterns for external validation, rather than independent risk factors or validated clinical diagnostic thresholds.

Abbreviations

AUC
area under the receiver operating characteristic curve
BMI
body mass index
CDI
Caton–Deschamps index
ICC
intraclass correlation coefficient

ISI
Insall–Salvati index
LASSO
least absolute shrinkage and selection operator
LTI
lateral trochlear inclination
MRI
magnetic resonance imaging
PACS
picture archiving and communication system
PTA
patellar tilt angle
PTI
patellotrochlear index
RF
random forest
SA
sulcus angle
SHAP
Shapley additive explanations
TFA
trochlear facet asymmetry
TGD
trochlear groove depth
TT–ME
tibial tubercle–midepicondyle distance
TT–TG
tibial tubercle–trochlear groove distance.

Declarations

Ethics approval and consent to participate

This retrospective case–control study was approved by the Institutional Review Board of the First Affiliated Hospital of Kunming Medical University(approval no.□2026□□□L□186□; approved on 9 June 2026). The requirement for written informed consent was waived by the Institutional Review Board because of the retrospective design and use of de-identified data. The study was conducted in accordance with the ethical principles of the Declaration of Helsinki and its subsequent amendments.

Consent for publication

Not applicable.

Availability of data and materials

The de-identified data supporting the findings of this study are not publicly available because they contain potentially identifiable clinical and imaging information. Data may be available from the corresponding author on reasonable request and subject to approval by the institutional review board.

Competing interests

The authors declare that they have no competing interests.

Funding

This study was supported by the The 2025 Undergraduate Innovation Training Program of Kunming Medical University (grant No.202510678062), the National Key Clinical Specialty Cultivation Project of Yunnan Province during the "14th Five-Year Plan" Period (grant No.300216), the Yunnan Fundamental Research Projects (grant NO. 202501AT070114),the ,and the Yunnan health training project of high level talents (No. H-2025064).The funders had no role in the study design, data collection, data analysis, interpretation of data, writing of the manuscript, or the decision to submit the manuscript for publication.

Authors' contributions

JHZ and MYZ contributed equally to this work. JHZ and MYZ contributed to conceptualization, methodology, data curation, formal analysis, investigation, validation, and writing of the original draft. JYZ contributed to data curation and validation. LZP contributed to methodology and formal analysis. XGY contributed to project administration and supervision. GFC contributed to conceptualization, supervision, and writing—review and editing. All authors read and approved the final manuscript.

References

1. Fithian DC, Paxton EW, Stone ML, Silva P, Davis DK, Elias DA, et al. Epidemiology and natural history of acute patellar dislocation. Am J Sports Med. 2004;32:1114–21. https://doi.org/10.1177/0363546503260788
2. Barbosa RM, da Silva MV, Macedo CS, Santos CP. Imaging evaluation of patellofemoral joint instability: a review. Knee Surg Relat Res. 2023;35:7. https://doi.org/10.1186/s43019-023-00180-8
3. Geraghty L, Humphries D, Fitzpatrick J. Assessment of the reliability and validity of imaging measurements for patellofemoral instability: an updated systematic review. Skeletal Radiol. 2022;51:2245–56. https://doi.org/10.1007/s00256-022-04110-9
4. Elias DA, White LM, Fithian DC. Acute lateral patellar dislocation at MR imaging: injury patterns of medial patellar soft-tissue restraints and osteochondral injuries of the inferomedial patella. Radiology. 2002;225:736–43. https://doi.org/10.1148/radiol.2253011578

5. Guerrero P, Li X, Patel K, Brown M, Busconi B. Medial patellofemoral ligament injury patterns and associated pathology in lateral patella dislocation: an MRI study. Sports Med Arthrosc Rehabil Ther Technol. 2009;1:17. https://doi.org/10.1186/1758-2555-1-17
6. Stenwig E, Salvi G, Rossi PS, Skjærvold NK. Comparative analysis of explainable machine learning prediction models for hospital mortality. BMC Med Res Methodol. 2022;22:53. https://doi.org/10.1186/s12874-022-01540-w
7. Nukala V, Sodhi A, Wadhavkar I, Mangudi Varadarajan K, Muratoglu O, Borjali A, et al. A Magnetic Resonance Imaging-Based Clinical Prediction Model Accurately Identifies Patellar Instability Risk Using Common Patellofemoral Measurements. Arthrosc Sports Med Rehabil. 2025;7:101159. https://doi.org/10.1016/j.asmr.2025.101159
8. Kwon HM, Nam J-H, Koh Y-G, Choi Y, Cho BW, Park KK, et al. Comparative Analysis of 3 Machine Learning Methods for Identifying Minimal Predictors of Patellofemoral Instability Risk Factors. Orthop J Sports Med. 2025;13:23259671251358390. https://doi.org/10.1177/23259671251358390
9. Nagawa K, Inoue K, Hara Y, Shimizu H, Tsuchihashi S, Matsuura K, et al. Three-dimensional magnetic resonance imaging-based statistical shape analysis and machine learning-based prediction of patellofemoral instability. Sci Rep. 2024;14:11390. https://doi.org/10.1038/s41598-024-62143-7
10. Haj-Mirzaian A, Thawait GK, Tanaka MJ, Demehri S. Diagnosis and Characterization of Patellofemoral Instability: Review of Available Imaging Modalities. Sports Med Arthrosc Rev. 2017;25:64–71. https://doi.org/10.1097/JSA.0000000000000148
11. Joseph SM, Cheng C, Solomito MJ, Pace JL. Lateral Trochlear Inclination Angle: Measurement via a 2-Image Technique to Reliably Characterize and Quantify Trochlear Dysplasia. Orthop J Sports Med. 2020;8:2325967120958415. https://doi.org/10.1177/2325967120958415
12. Kim HK, Parikh S. Patellofemoral Instability in Children: Imaging Findings and Therapeutic Approaches. Korean J Radiol. 2022;23:674–87. https://doi.org/10.3348/kjr.2021.0577
13. Biedert RM, Albrecht S. The patellotrochlear index: a new index for assessing patellar height. Knee Surg Sports Traumatol Arthrosc. 2006;14:707–12. https://doi.org/10.1007/s00167-005-0015-4
14. Macri EM, Felson DT, Zhang Y, Guermazi A, Roemer FW, Crossley KM, et al. Patellofemoral morphology and alignment: reference values and dose-response patterns for the relation to MRI features of patellofemoral osteoarthritis. Osteoarthritis Cartilage. 2017;25:1690–7. https://doi.org/10.1016/j.joca.2017.06.005
15. Skelley N, Friedman M, McGinnis M, Smith C, Hillen T, Matava M. Inter- and intraobserver reliability in the MRI measurement of the tibial tubercle-trochlear groove distance and trochlea dysplasia. Am J Sports Med. 2015;43:873–8. https://doi.org/10.1177/0363546514565768
16. Iseki T, Nakayama H, Daimon T, Kambara S, Kanto R, Yamaguchi M, et al. Tibial Tubercle-Midepicondyle Distance Can Be a Better Index to Predict the Outcome of Medial Patellofemoral Ligament Reconstruction Than Tibial Tubercle-Trochlear Groove Distance. Arthrosc Sports Med Rehabil. 2020;2:e697–704. https://doi.org/10.1016/j.asmr.2020.04.014

17. Singerman R, Davy DT, Goldberg VM. Effects of patella alta and patella infera on patellofemoral contact forces. J Biomech. 1994;27:1059–65. https://doi.org/10.1016/0021-9290(94)90222-4
18. Escala JS, Mellado JM, Olona M, Giné J, Saurí A, Neyret P. Objective patellar instability: MR-based quantitative assessment of potentially associated anatomical features. Knee Surg Sports Traumatol Arthrosc. 2006;14:264–72. https://doi.org/10.1007/s00167-005-0668-z
19. Gobbi RG, Cavalheiro CM, Giglio PN, Hinckel BB, Camanho GL. Patellar Tilt and Patellar Tendon-Trochlear Groove Angle Present the Optimum Magnetic Resonance Imaging Diagnostic Reliability for Patients With Patellar Instability. Arthroscopy. 2023;39:2339–51. https://doi.org/10.1016/j.arthro.2023.04.005
20. Siontis GCM, Tzoulaki I, Castaldi PJ, Ioannidis JPA. External validation of new risk prediction models is infrequent and reveals worse prognostic discrimination. J Clin Epidemiol. 2015;68:25–34. https://doi.org/10.1016/j.jclinepi.2014.09.007
21. Collins GS, Moons KGM, Dhiman P, Riley RD, Beam AL, Van Calster B, et al. TRIPOD+AI statement: updated guidance for reporting clinical prediction models that use regression or machine learning methods. BMJ. Clinical research ed.; 2024;385:e078378. https://doi.org/10.1136/bmj-2023-078378
22. Fabricant PD, Heath MR, Mintz DN, Emery K, Veerkamp M, Gruber S, et al. Many Radiographic and Magnetic Resonance Imaging Assessments for Surgical Decision Making in Pediatric Patellofemoral Instability Patients Demonstrate Poor Interrater Reliability. Arthroscopy. 2022;38:2702–13. https://doi.org/10.1016/j.arthro.2022.03.033

Figures

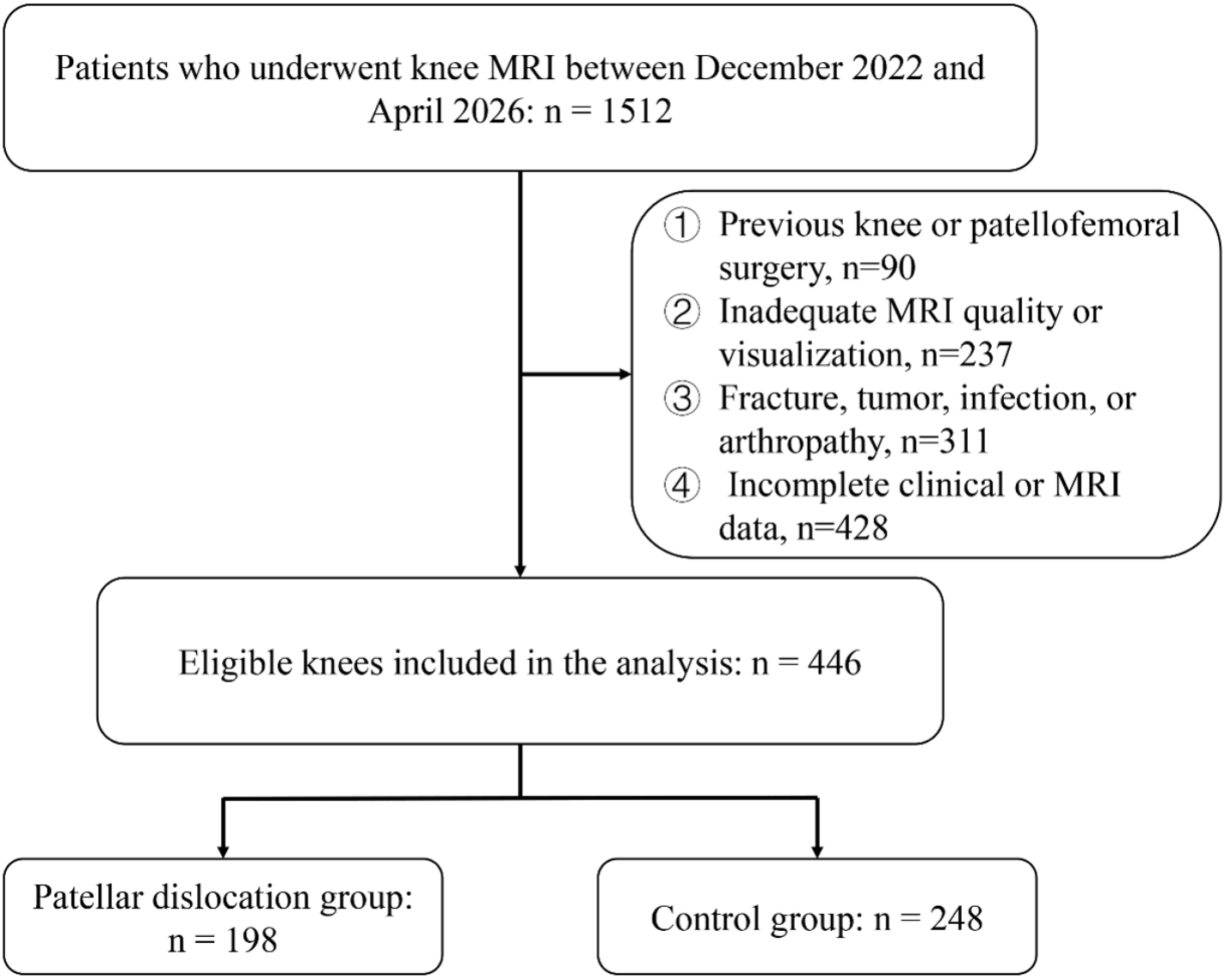


Figure 1

Flow diagram of study population selection.

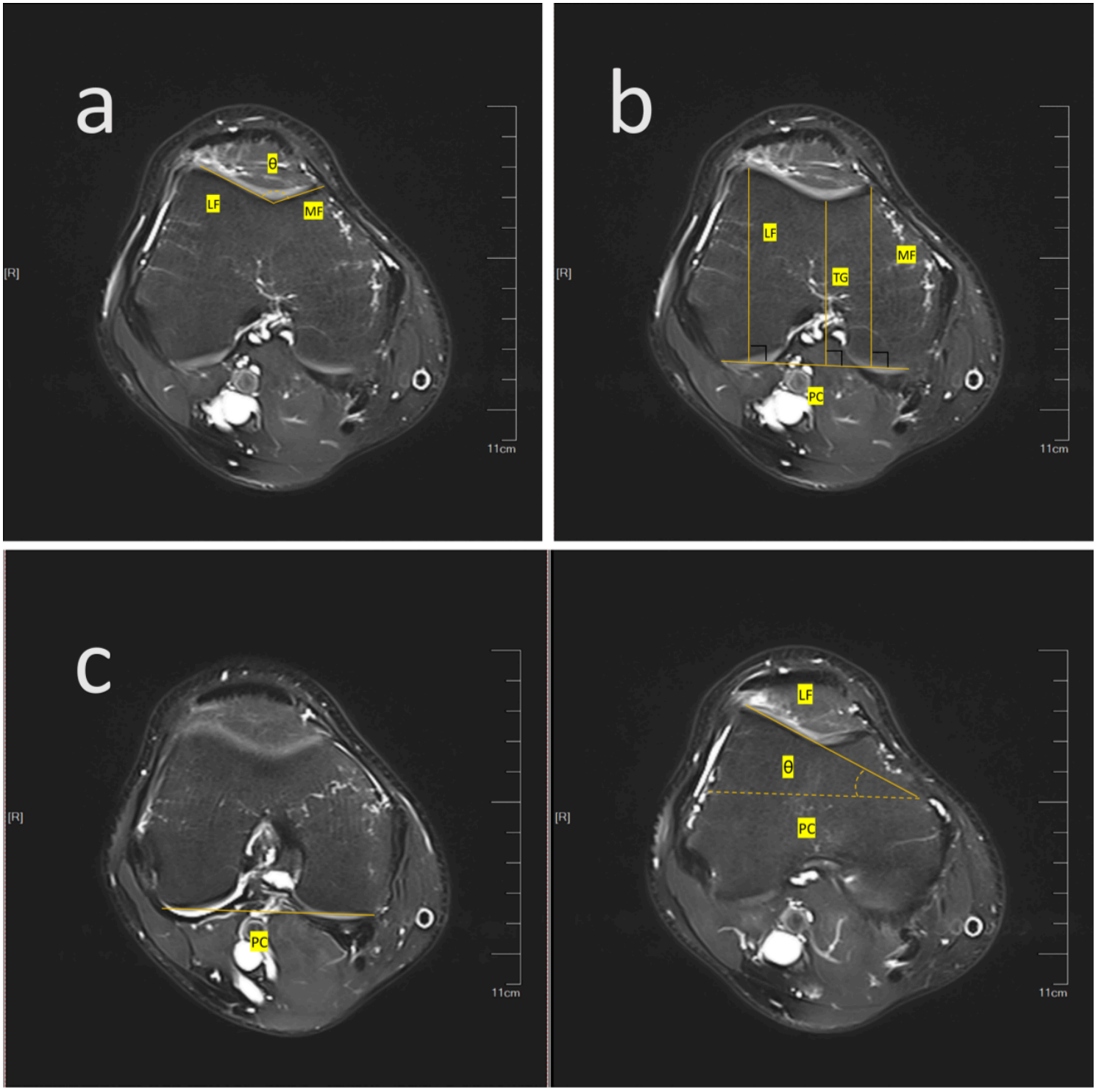


Figure 2

a Sulcus angle (∠θ) and trochlear facet asymmetry (MF/LF). b Trochlear groove depth ((MF+LF)/2−TG) c Lateral trochlear inclination (∠θ).



Figure 3

a Insall–Salvati Index (T/P). b Caton–Deschamps Index (T/P). c Patellotrochlear Index (F/P)

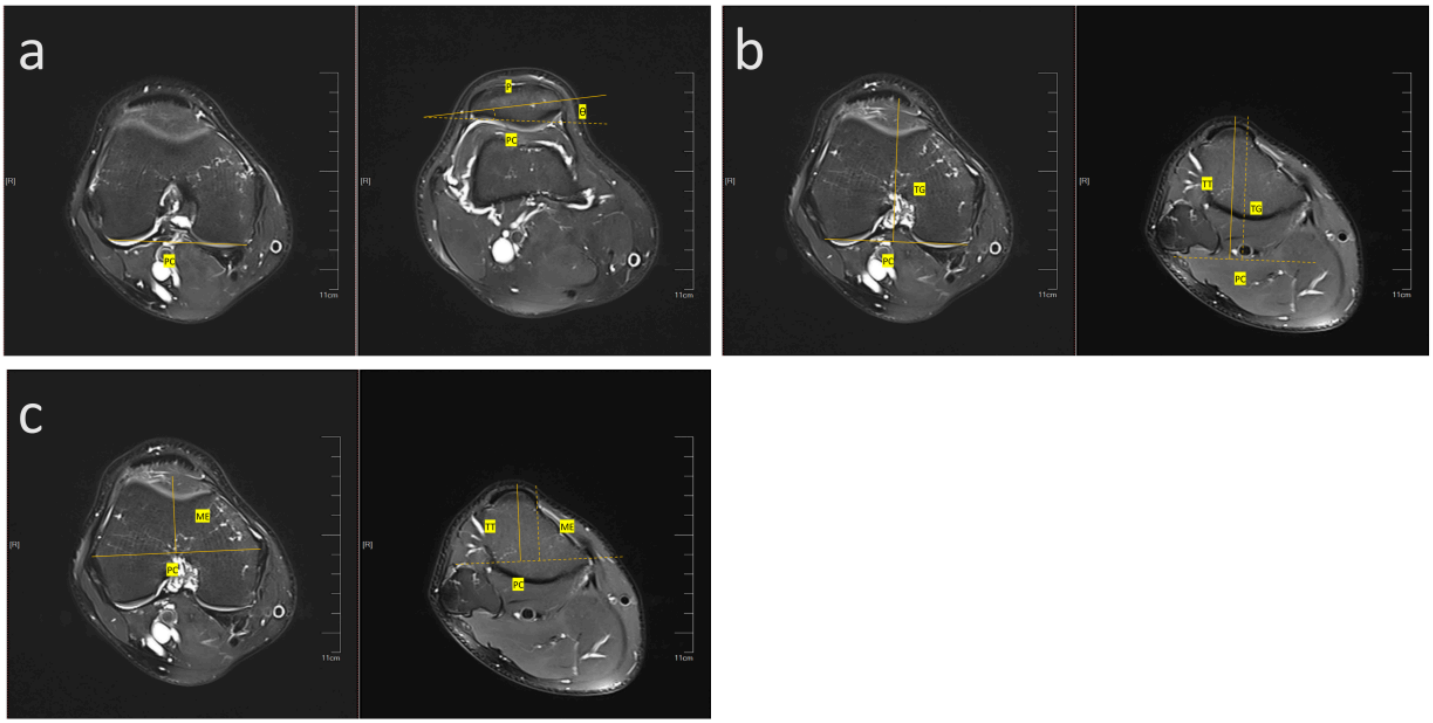


Figure 4

a Patellar tilt angle (∠θ).b Tibial tubercle–trochlear groove distance (distance TT–TG).c Tibial tubercle-Midepicondyle Distance((distance TT–ME)

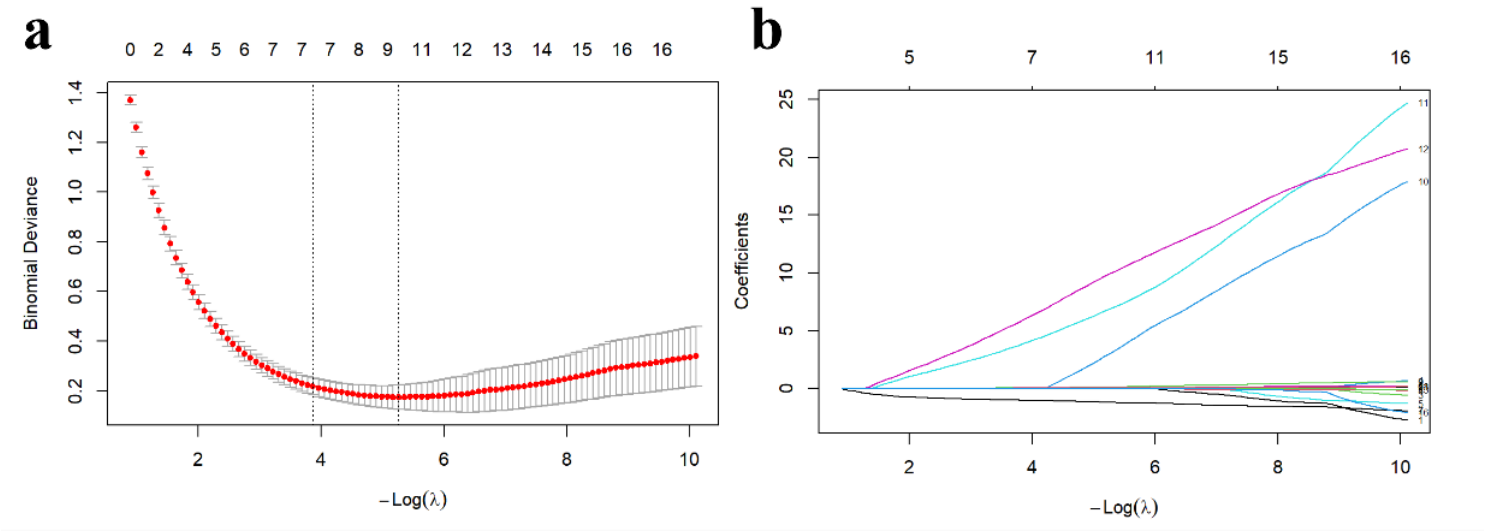


Figure 5

LASSO feature selection in the training set.

(a) Ten-fold cross-validation curve for selection of the regularization parameter λ. Red points represent the mean cross-validated binomial deviance, and gray error bars indicate ±1 standard error. The two vertical dashed lines correspond to λ.1se and λ.min. (b) LASSO coefficient profiles of the candidate variables across different values of λ. Each curve represents one candidate variable, and the numbers along the upper axes indicate the number of nonzero coefficients. Using the λ.1se criterion, seven variables with nonzero coefficients were retained: TGD, TFA, SA, CDI, ISI, PTA, and TT–TG distance. LASSO, least absolute shrinkage and selection operator.

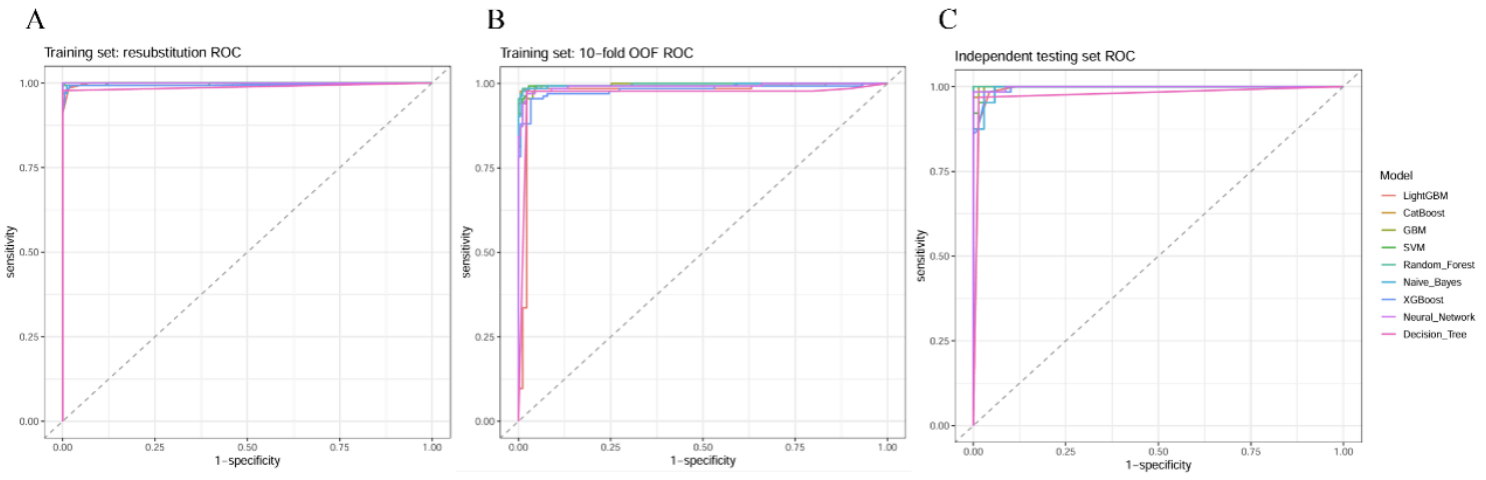


Figure 6

Receiver operating characteristic curves of nine machine learning models for classifying patellar dislocation.

Receiver operating characteristic curves for LightGBM, CatBoost, GBM, support vector machine, random forest, naive Bayes, XGBoost, neural network, and decision tree in the training-set resubstitution analysis (A), 10-fold out-of-fold analysis (B), and independent testing set (C). AUC, area under the receiver operating characteristic curve; OOF, out-of-fold; GBM, gradient boosting machine.

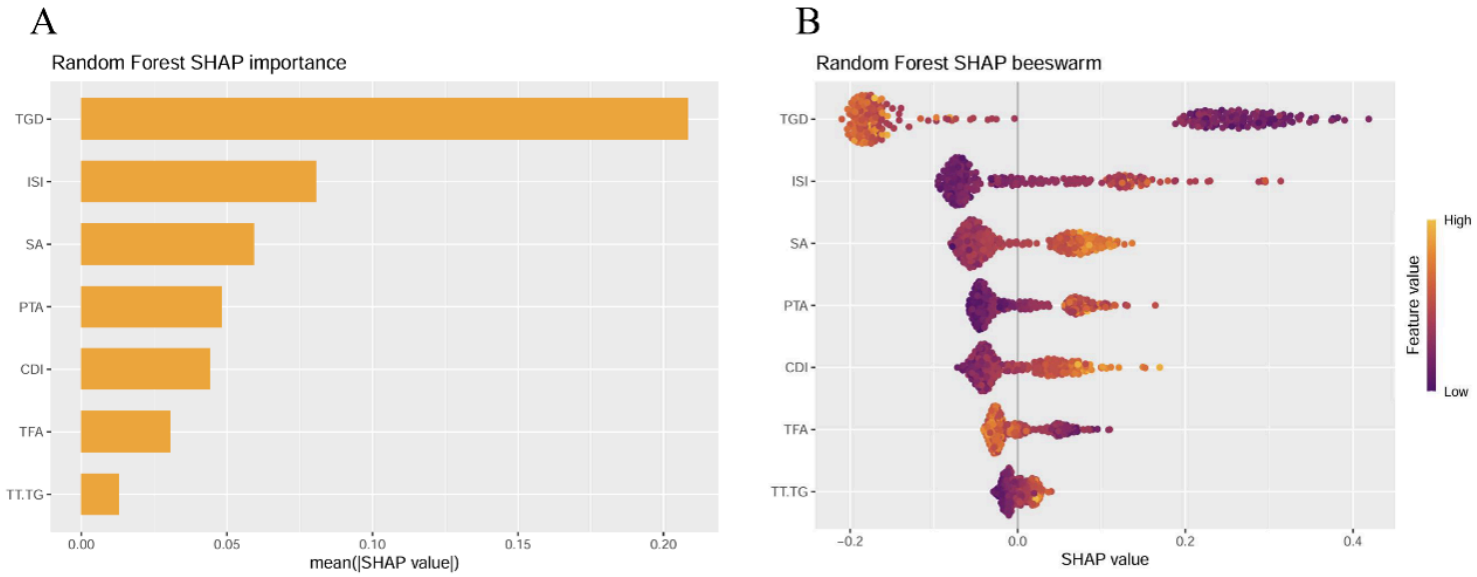


Figure 7

SHAP-based interpretation of the random forest model.

(A) Global feature importance ranked by mean absolute SHAP value. (B) SHAP summary plot showing the direction and distribution of feature contributions. Each point represents one participant, and color indicates the feature value from low (purple) to high (orange). Positive SHAP values favor patellar dislocation. SHAP, Shapley additive explanations.

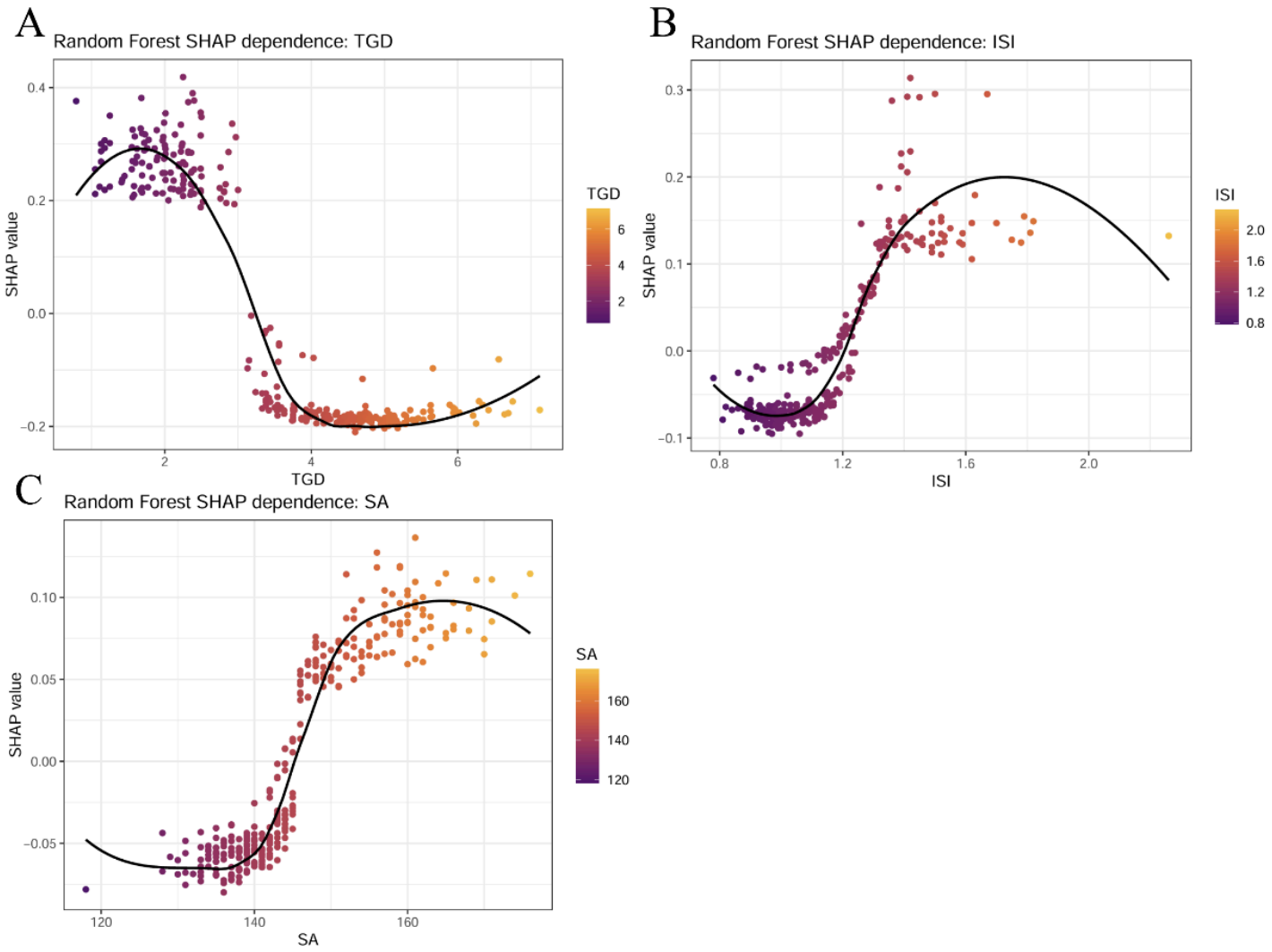


Figure 8

SHAP dependence plots for the leading variables in the random forest model.

Dependence plots show the contribution patterns of TGD (A), ISI (B), and SA (C). Each point represents one participant, and the black curve shows the smoothed trend. Positive SHAP values favor patellar dislocation. SHAP, Shapley additive explanations; TGD, trochlear groove depth; ISI, Insall–Salvati index; SA, sulcus angle.

Supplementary Files

This is a list of supplementary files associated with this preprint. Click to download.

- SupplementaryTable1.csv
- SupplementaryFigure1.tiff